Biomech Model Mechanobiol
DOI 10.1007/s10237-013-0506-z

ORIGINAL PAPER

Cellular contractility and substrate elasticity: a numerical investigation of the actin cytoskeleton and cell adhesion

William Ronan · Vikram S. Deshpande · Robert M. McMeeking · J. Patrick McGarry

Received: 18 January 2013 / Accepted: 1 June 2013

Abstract Numerous experimental studies have established that cells can sense the stiffness of underlying substrates and have quantified the effect of substrate stiffness on stress fibre formation, focal adhesion area, cell traction, and cell shape. In order to capture such behaviour, the current study couples a mixed mode thermodynamic and mechanical framework that predicts focal adhesion formation and growth with a material model that predicts stress fibre formation, contractility, and dissociation in a fully 3D implementation. Simulations reveal that SF contractility plays a critical role in the substrate-dependent response of cells. Compliant substrates do not provide sufficient tension for stress fibre persistence, causing dissociation of stress fibres and lower focal adhesion formation. In contrast, cells on stiffer substrates are predicted to contain large amounts of dominant stress fibres. Different levels of cellular contractility representative of different cell phenotypes are found to alter the range of substrate stiffness that cause the most significant changes in stress fibre and focal adhesion formation. Furthermore, stress fibre and focal adhesion formation evolve as a cell spreads on a substrate and leading to the formation of bands of fibres leading from the cell periphery over the nucleus. Inhibiting the formation of FAs during cell spreading is found to limit stress fibre formation. The predictions of this mutually dependent material-interface framework are strongly supported by experimental observations of cells adhered to elastic substrates and offer insight into the inter-dependent biomechanical processes regulating stress fibre and focal adhesion formation.

Keywords Stress fibre contractility · Focal adhesion formation · Substrate elasticity · Nucleus stress · Finite element · Active constitutive formulation

Electronic supplementary material The online version of this article (doi:10.1007/s10237-013-0506-z) contains supplementary material, which is available to authorized users.

W. Ronan · J. P. McGarry (✉)
Department of Mechanical and Biomedical Engineering, National University of Ireland Galway, University Road, Galway, Ireland
e-mail: patrick.mcgarry@nuigalway.ie

W. Ronan
e-mail: w.ronan1@nuigalway.ie

V. S. Deshpande
Department of Engineering, University of Cambridge, Trumpington Street, Cambridge CB2 1PZ, UK
e-mail: vsd@eng.cam.ac.uk

R. M. McMeeking
Departments of Mechanical Engineering Materials, University of California, Santa Barbara, CA 93106-5070, USA
e-mail: rmcm@engineering.ucsb.edu

R. M. McMeeking
School of Engineering, University of Aberdeen King's College, Aberdeen AB24 3UE, Scotland, UK

1 Introduction

Previous experimental studies have established that cells can sense the stiffness of underlying substrates and that cellular tractions depend on substrate stiffness (Tee and Fu 2011; Discher and Janmey 2005). Substrate stiffness has also been shown to direct stem cell lineage specification (Engler et al. 2006) and affect cell motility (Lo et al. 2000). The contractile response of cells to ECM stiffness has been shown to be an important factor in wound healing (Danjo and Gipson 1998), atherosclerosis (Isenberg et al. 2009), and cancer progression (Paszek et al. 2005; Levental et al. 2009).

Changes in substrate stiffness have been shown to significantly alter the actin cytoskeleton and focal adhesions

Published online: 18 June 2013

(FAs) of a range of cell types, including fibroblasts, mesenchymal stem cells, endothelial cells, and chondrocytes (Goffin et al. 2006; Engler et al. 2006; Byfield et al. 2009; Schuh et al. 2010). Different ranges of substrate stiffness that influence cytoskeletal remodelling have been reported for different cell phenotypes; particularly, more contractile cells, such as myoblasts, are most sensitive up to ∼400 kPa (Ren et al. 2008), but less contractile cells, such as fibroblasts, are sensitive up to ∼20 kPa (Yeung et al. 2005). Previous in vitro studies have quantified the effect of different substrate stiffness on stress fibre (SF) formation (Solon et al. 2007), FA area (Goffin et al. 2006), cell traction (Califano and Reinhart-King 2010), and cell shape (Yeung et al. 2005). However, the cellular mechanisms underlying these phenomena are poorly understood. Experimental observations of cells adhered to micropatterned surfaces have previously been combined with numerical analyses to investigate this substrate sensing phenomena (McGarry et al. 2009); however, these investigations were not performed for continuous elastic substrates. In order to provide insight into the role of the contractile cytoskeleton and cellular adhesions, it is necessary to employ an active constitutive formulation for them that considers the remodelling and contractility of the cytoskeleton in tandem with the formation of FAs in a fully three-dimensional framework.

Previously, the contractile cytoskeleton has been included in computational models of biological gels as prepositioned passive filaments with prescribed shrinkage strains (Mohrdieck et al. 2005; Storm et al. 2005). However, these studies offer limited insight as they do not consider the underlying cellular processes. More recently, models have been proposed that consider contractility and remodelling of the cytoskeleton using different approaches: Vernerey and Farsad (2011) assume that the rate of SF formation is increased by fibre tension; the model of Kaunas and Hsu (2009) assumes that the rate of fibre dissociation increases as the fibre strain deviates from an optimal level. A more recent study by Kaunas et al. (2011) assumes that fibre dissociation is related to the fibre strain rate. Deshpande et al. (2007) propose a computational model based on the biochemistry of the actin cytoskeleton; SF formation is driven by an activation signal, dissociation is triggered by a drop in fibre tension, and SF contractility is captured using a Hill-type law. This model has previously been used in 2D to investigate cells adhered to patterned substrates and micropost arrays (McGarry et al. 2009; Pathak et al. 2008). Recently, this material formulation has been implemented in a 3D framework to demonstrate that the increased compression resistance of spread cells is due to SF contractility (Ronan et al. 2012).

FAs provide a mechanical link between the cytoskeleton and a substrate or extracellular matrix and also play an important role in cellular signalling (Wang 2000; Schwartz et al. 1995). FA formation is modulated by traction forces on the adhesion, and the size of the adhesion increases with force (Tan et al. 2003; Balaban et al. 2001). FAs are typically observed experimentally at the end of SF bundles (Burridge et al. 1988), and disrupting SF contractility has been shown to cause FAs to disappear (Oakes et al. 2012). Previous attempts to simulate FA dynamics have not considered the coupling between active SF contractility and FA assembly (Shemesh et al. 2005; Bruinsma 2005). A study by Deshpande et al. (2008) presents a coupled thermodynamic and mechanical framework that incorporates SF formation kinetics, SF contractility, and the force sensitivity of FA formation and growth. This framework captures the experimentally observed inter-dependence between SFs and FAs via the Hill-like contractility of SFs and thermodynamic equilibrium of FA integrins. This formulation has been used previously to accurately predict the formation of SFs and FAs for cells adhered to concave- and convex-shaped ligand patterns (Pathak et al. 2008) for idealised 2D geometries.

In the current study, the FA interaction model of Deshpande et al. is expanded to include both specific and non-specific adhesion dynamics. This expanded model is implemented in a mixed mode formulation that allows for both normal and tangential stretching of FA bonds between the cell and substrate. This mixed mode interface formulation is employed with the 3D SF implementation of Ronan et al. to examine the effect of substrate stiffness on SF and FA formation (Deshpande et al. 2007, 2006; Ronan et al. 2012). The current study builds upon previous applications of the SF framework (Pathak et al. 2012; McGarry et al. 2009; Ronan et al. 2012); previous studies have not considered mixed mode FA behaviour, passive/non-specific adhesion forces, cell spreading, or cells adhered to elastic substrates in a 3D environment. We also show changes in cell shape, nucleus stress, and cell tractions with substrate stiffness. We investigate the effect of different levels of contractility associated with a range of cell phenotypes when seeded on elastic substrates. Finally, we examine the role of SF and FA formation, including the sliding of FA bonds, in the spreading of cells by considering a cell that is not initially in contact with a substrate.

2 Materials and methods

2.1 SF biochemistry

The contractile actin–myosin cytoskeleton is formed via the phosphorylation of myosin and polymerization of actin filaments. The myosin self assembles into bipolar filaments that interact with actin filaments which are loosely bound with α-actinin to form contractile actin–myosin bundles. The formation and behaviour of stress fibres (SFs) consists of three couple phenomena: SF formation is triggered by an activation signal; reduction in fibre tension leads to fibre dissociation;

the contractile behaviour of SFs is similar to the Hill model for muscle (Hill 1938).

As described previously by Deshpande et al. (2006), these phenomena are captured in our material model via two key equations. First, the tension in the SF bundle, which is generated by cross-bridge cycling of actin–myosin pairs (Warshaw et al. 1990), is related to the bundle contraction rate using the following Hill-like equation:

$$\frac{\sigma_f}{\sigma_0} = \begin{cases} 0 & \frac{\dot{\varepsilon}}{\dot{\varepsilon}_0} \leq -\frac{\eta}{\bar{k}_v} \\ 1 + \frac{\bar{k}_v}{\eta}\frac{\dot{\varepsilon}}{\dot{\varepsilon}_0} & -\frac{\eta}{\bar{k}_v} \leq \frac{\dot{\varepsilon}}{\dot{\varepsilon}_0} \leq 0 \\ 1 & \frac{\dot{\varepsilon}}{\dot{\varepsilon}_0} > 0 \end{cases} \quad (1)$$

where σ_f is the stress in the SF bundle, σ_0 is the isometric tension, and $\bar{k}_v$ is the reduction in stress upon increasing the shortening strain rate, $\dot{\varepsilon}$, by a reference strain rate $\dot{\varepsilon}_0$. The dimensionless activation level of a SF bundle, η $(0 \leq \eta \leq 1)$, at any orientation, also defines the isometric tension, σ_0, where $\sigma_0 = \eta\sigma_{\max}$. $\sigma_{\max}$ is the maximum tension in a fully activated bundle.

Second, the signal-induced formation and tension-dependent dissociation of the actin cytoskeleton are captured using a first-order kinetic equation:

$$\frac{\mathrm{d}\eta}{\mathrm{d}t} = [1-\eta]\frac{C\bar{k}_f}{\theta} - \left(1 - \frac{\sigma_f}{\sigma_0}\right)\eta\frac{\bar{k}_b}{\theta} \quad (2)$$

The first term on the right of the equality governs the rate of formation of the SFs and is controlled by the dimensionless constant $\bar{k}_f$, the signal C, and decay constant θ. The latter part of the equation gives the rate of dissociation and is governed by the dimensionless constant $\bar{k}_b$, the stress level σ_f, and the isometric tension σ_0.

2.2 Cell adhesion dynamics

Cell-substrate interactions can be considered as active/specific interactions that involve binding proteins and passive/non-specific interactions such as electrostatic tractions, van der Waals interactions, hydrophobic forces, and steric repulsion (Bell 1978; Cheng et al. 2009). In the current study, passive forces are considered in the normal direction only and active forces are considered in both the normal and shear directions using a mixed mode formulation (Fig. 1). These passive forces are averaged over the entire membrane area giving the passive traction, but are assumed to act only on the portion of the membrane excluding the area covered by integrins, as shown in Fig. 2g. Therefore, passive forces acting directly on integrins are neglected, as the area associated with each integrin is small compared to the surface area of the cell not covered by integrins. The inclusion of such passive traction is motivated by the studies of Leckband et al. (1992, 2001) with long range attractive forces being observed experimentally. Cheng et al. (2009) have also used non-specific long range forces to facilitate the formation of specific forces after the ligands and integrins are sufficiently close. The passive traction is defined in rela-

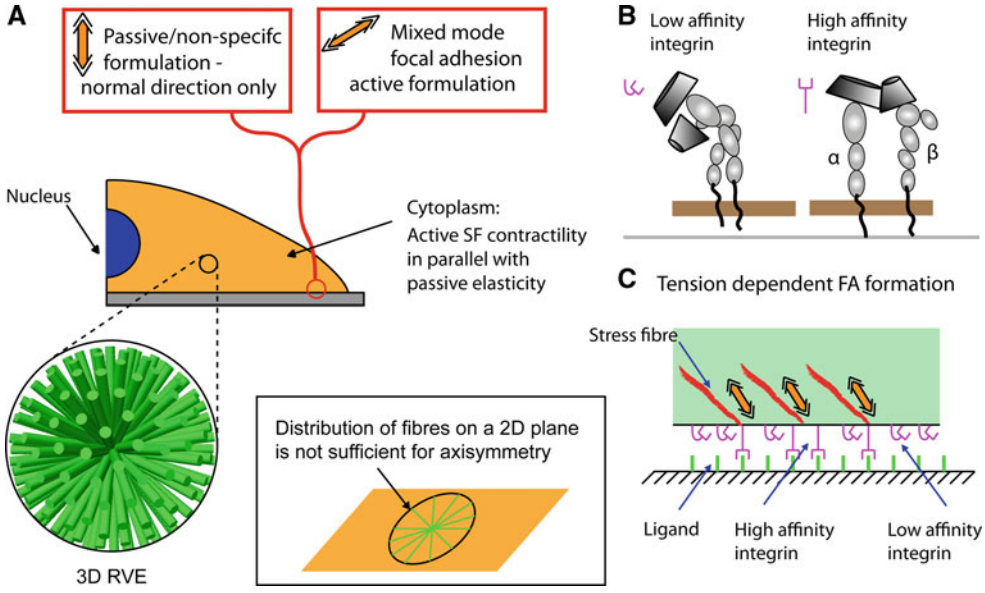

Fig. 1 **a** Schematic diagram of a 3D cell showing cell in yellow and the nucleus shown in blue. Inset shows 240 fibre orientations in 3D space within the representative volume element (RVE). The 3D fibre implementation may be used with an axisymmetric geometry; however, it should be noted that it is insufficient to restrict SF orientations to a 2D plane (as shown *bottom* right) when considering an axisymmetric geometry. A mixed mode focal adhesion formulation is used together with a passive or non-specific formulation to simulate the interaction between the cell and substrate. **b** High affinity and low affinity integrins involved in the formation of focal adhesions. **c** Bound and unbound integrins between a cell containing stress fibres and a ligand-coated substrate

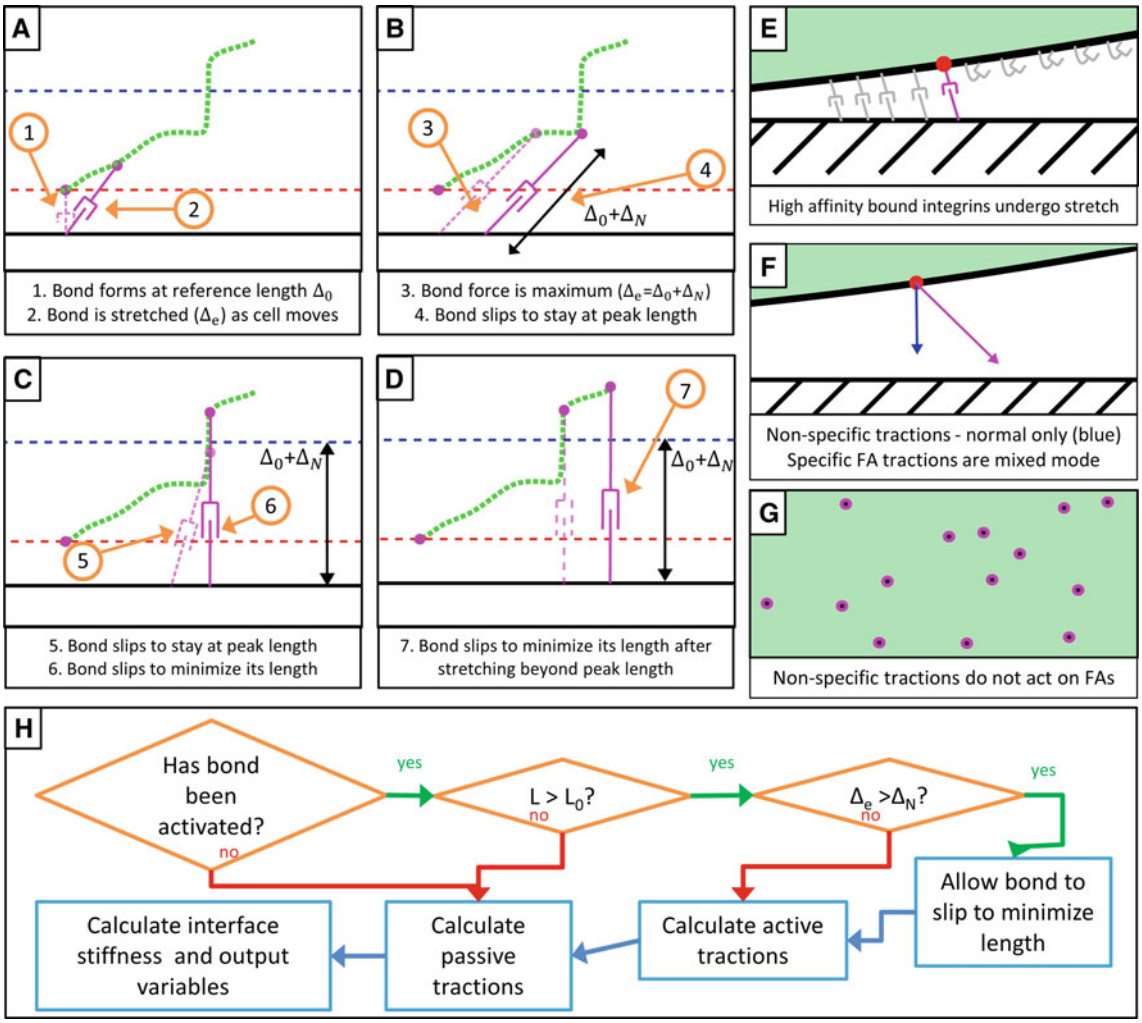

Fig. 2 **a–d** The evolution of a single integrin-ligand bond undergoing stretch. *1* Bond forms at reference length Δ_0. *2* Bond is stretched by relative movement between the cell and substrate. *3* Bond reaches length $\Delta_n + \Delta_0$, at which the bond force is at a maximum (*Note* This length is shown as a *black line with arrows*). *4*, *5* Bond slips to stay at peak length. *6*, *7* Bond slips to minimize its length after stretching beyond peak length. **e** Node on the cell surface (shown in *red*) where an integrin-ligand bond has formed and is under stretch. **f** The active (*pink*) and passive (*blue*) tractions acting on the cell. The active (specific) component is a result of mixed mode deformation. In contrast, the passive (non-specific) component acts in the normal direction only. **g** View of the cell surface. In order to simplify the thermodynamic analysis of the active bond, the passive or non-specific tractions are assumed to act on the surface of the cell only, and not on bound integrins (the area shown in *green*). The area covered by active integrins (shown in *pink*) is assumed to be small, and therefore, the area subjected to the non-specific tractions is assumed to be equal to the entire cell area

tion to the normal separation distance Δ_1 using the following equation:

$$T_1^P = \varphi_0^P \frac{\Delta_1}{\delta_p^2} e^{-\frac{\Delta_1}{\delta_P}} \tag{3}$$

where δ_P is the passive characteristic distance and φ_0^P is the passive interaction potential. The form of this equation is based on the observations of Leckband and Israelachvili (2001) for non-specific tractions such as van der Waals', electrostatic, and hydrophobic forces.

The formation of active/specific adhesions of cells to a substrate is simulated using a recent thermodynamically motivated model (Deshpande et al. 2008). This model considers the formation of FAs via the bonding of integrins on the cell surface to suitable ligands on the ECM. Binding integrins on the cell surface exist in two conformational states: high affinity, or "straight," integrins with a high reference chemical potential, μ_H, and low affinity, or "bent", integrins with lower reference chemical potential, μ_L. Only the high affinity integrins form bonds and low affinity integrins remain unbonded (Fig. 1). Low affinity integrins with a concentration ξ_L have chemical potential:

$$\chi_L = \mu_L + kT \ln\left(\frac{\xi_L}{\xi_0}\right) \tag{4}$$

where μ_L accounts for enthalpy and the last term for configurational entropy. ξ_0 is the total concentration of integrins, and k and T are the Boltzmann constant and the absolute temperature.

High affinity integrins form bonds and undergo stretching; therefore, the potential energy stored in the bond is accounted for in the chemical potential as:

$$\chi_H = \mu_H + kT\ln\left(\frac{\xi_H}{\xi_0}\right) + \Phi\left(\Delta_i\right) - F_i\Delta_i \tag{5}$$

where Φ is the stretch energy and $F_i\Delta_i$ is the potential energy of the applied force F_i. The force F_i is related to the stretch by:

$$F_i = \frac{\partial\Phi}{\partial\Delta_i} \tag{6}$$

The kinetics of bond formation and the diffusion of low affinity integrins along the cell membrane are considered fast compared with other time scales. Therefore, diffusive kinetics are neglected, and the total concentration of integrins, i.e., the low plus the high affinity ones, is held fixed at ξ_0 everywhere on the membrane. Similarly, the kinetics of bond formation is so rapid that we can use thermodynamic equilibrium, $\chi_H = \chi_L$, to obtain the individual concentrations of high and low affinity integrins as:

$$\xi_H = \frac{\xi_0}{\exp\left[\frac{\mu_H-\mu_L+\Phi-F_i\Delta_i}{kT}\right]+1} \tag{7}$$

$$\xi_L = \frac{\xi_0}{\exp\left[-\frac{\mu_H-\mu_L+\Phi-F_i\Delta_i}{kT}\right]+1} \tag{8}$$

The stretch energy Φ is expressed as a piecewise quadratic potential:

$$\Phi = \begin{cases} \kappa_s\Delta_e^2 & \Delta_e \le \Delta_n \\ -\kappa_s\Delta_n^2 + 2\kappa_s\Delta_n\Delta_e - \kappa_s\Delta_e^2 & \Delta_n < \Delta_e \le 2\Delta_n \\ \kappa_s\Delta_n^2 & \Delta_e > 2\Delta_n \end{cases} \tag{9}$$

where κ_s is the stiffness of the bond; Δ_e is the effective stretch; and Δ_n is the peak bond length.

2.3 Representation of cellular signalling

In the current study, the complete signalling pathway, which is more rigorously described by Pollard et al. (2000) and Zeng et al. (2011), is not considered. The kinetics of the signalling pathway and the proteins involved are not dealt with. Instead, a simplified spatially uniform signal is used to represent all signalling pathways associated with contractility. In computations where the spreading of the cell on a rigid surface is simulated, the cell geometry changes during spreading and adhesions are continuously activated; therefore, a spatially uniform continuous signal ($C = 1$) is used to represent continuous activation of stretch-activated channels. In contrast, the computations involving predefined cell geometries adhered to elastic substrates do not result in significant deformation during the simulation, and adhesion activation is not sustained; therefore, a spatially uniform exponentially decaying signal is used ($C = \exp(-t/\theta)$).

2.4 Numerical implementation

2.4.1 Material model

Fibre formation is considered in a fully 3D environment, with fibres allowed to form in any direction at every point in a 3D geometry. The number of calculation points may be reduced by assuming that the geometry is axisymmetric; however, it should be noted that for axisymmetric simulations, it is necessary to consider 3D orientations of fibres. It is not correct to restrict SF orientations to the axisymmetric plane. As previously described by Ronan et al. (2012), the material model is implemented in a 3D framework (Fig. 1). The active stress is calculated by summing the contributions of each fibre. Each fibre stress is calculated based on the kinetic and contractility equations described above. The stress tensor in the Cartesian basis generated by the active SF contractility is given as:

$$\sigma_{ij}^A = \sum_{k=1}^{n}\frac{\sigma_f\left(\omega_k,\varphi_k\right)}{n} m\left(\omega_k,\varphi_k\right)_i m\left(\omega_k,\varphi_k\right)_j \tag{10}$$

where n is the number of fibre orientations and the vector $m = \sin(\omega)\cos(\varphi)\,x_1 + \sin(\omega)\sin(\varphi)\,x_2 + \cos(\omega)\,x_3$ describes the orientation of the fibres in 3D space.

In parallel to the active SF behaviour described above, the passive material surrounding the SFs in the cell cytoplasm is modelled using a compressible neo-Hookean hyperelastic formulation, whereby the passive stress tensor is given as:

$$\sigma_{ij}^P = \frac{2}{J}C_{10}\left(\frac{B_{ij}}{J^{2/3}} - \frac{1}{3}\frac{B_{kk}\delta_{ij}}{J^{2/3}}\right) + \frac{2}{D_1}(J-1) \tag{11}$$

where B is the left Cauchy–Green tensor, J is the Jacobian of the deformation gradient, and C_{10} and D_1 are elasticity constants.

The complete stress state at any point in the cell cytoplasm is then given as:

$$\sigma_{ij} = \sigma_{ij}^A + \sigma_{ij}^P \tag{12}$$

This active constitutive formulation is implemented as a *user-defined material subroutine* in the commercial software Abaqus (Dassault Systemes, RI). The cell nucleus is modelled as a passive hyperelastic material using the same formulation given in Eq. (11). The subscripts "$_{cyto}$," "$_{nuc}$," and "$_{sub}$" are used to denote material properties for the cytoplasm, nucleus, and substrate, respectively.

2.4.2 Interaction model

The concentration of bound integrins, ξ_H, and the stretch energy, Φ, both depend on the effective stretch of the integrin-ligand bond, Δ_e. The effective stretch is based on the movement between the cell and the substrate. However, a bond forms at a non-zero length Δ_0, and it is possible for a bond to slip when an bound integrin jumps to a nearby ligand. A bond will slip if doing so would lower its chemical potential χ_H, i.e., if it is stretched past its peak length, Δ_n, and there is a suitable available ligand. The evolution of a single bond is shown below in Fig. 2. The effective stretch is defined as

$$\Delta_e = \sqrt{\Delta_1^2 + \Delta_2^2} - \Delta_0 \tag{13}$$

where Δ_1 and Δ_2 are the normal and tangential stretch components.

The tractions on the cell surface depend on the force (F_i) on each bond and the concentration of bound high affinity integrins (ξ_H) such that:

$$T_1 = -\xi_H F_1 - T_1^P, \quad T_2 = -\xi_H F_2 \tag{14}$$

These tractions are balanced by stresses in the cell caused by cellular contractility such that:

$$\sigma_{ij} n_j = T_i \tag{15}$$

where σ_{ij} is the Cauchy stress in the cell and n_j is the surface normal.

2.4.3 Finite element simulations

A finite element mesh was generated for a spread cell in contact with an elastic substrate and for a cell that is initially not in contact with a rigid substrate. In both cases, axisymmetric geometries are assumed, as shown in Fig. 1. Each finite element model consists of 3 sections with different material models: the substrate is modelled as an elastic material; the cell nucleus is modelled as hyperelastic material; and the cytoplasm is modelled using the active formulation defined above. The cytoplasm and nucleus are continuous, and no slip is permitted between the nucleus and cytoplasm. The contact interaction between cell and the substrate is simulated using the mixed mode FA formulation defined above. The material and interaction formulations are implemented in the finite element software Abaqus (Dassault Systemes, RI) as a *user-defined interface (UINTER)* and *user-defined material (UMAT)*, respectively. A mesh sensitivity study was performed, and no changes to the results were observed for smaller element sizes. The simulations consist of a single analysis step: for the cell adhered to the elastic substrate, SF formation is driven by an exponentially decaying signal; for the cell spreading on the rigid substrate, SF formation and the spreading process are driven by a constant signal.

2.5 Model parameters and interpretation of results

The material parameters used in the current study are based on previous implementations of the current formulation which were used to simulate cells adhered to microposts and cells under direct shear (McGarry et al. 2009; Dowling et al. 2012). In order to investigate the role of contractility, three representative cell types are selected: smooth muscle cells (SMCs), fibroblasts (FBs), and chondrocytes (CH). The contractility of these cells is captured by setting the value of $\sigma_{\max}$ to 25, 3.5, and 0.85 for SMCs, FBs, and CHs respectively, based on the studies of Dowling et al. (2012) and McGarry et al. (2009). A passive cytoplasm stiffness of $E_{\text{cell}} = 0.4$ kPa and a nucleus stiffness of 4.0 kPa are chosen for all cell types, and the additional active parameters (i.e., the signal decay time constant, the hill constant, the forwards and backwards kinetic constants, and the reference strain rate) are set to $\theta = 70$ s, $k_v = 7, k_f = 10, k_b = 1, \dot{\varepsilon}_0 = 0.003$ s^{-1}. The parameters for the FA model are chosen based on previous calibrations of this model (Deshpande et al. 2008; Pathak et al. 2008) as: $(\mu_H - \mu_L) = 2.14 \text{ x } 10^{-20}$ J; $\xi_0 = 200\,\mu\text{m}^{-2}$; $\kappa_s = 0.15\text{nN}\,\mu\text{m}^{-1}$; $\Delta_n = 0.13\,\mu$m. The parameters of the passive component of the interface model are: $\delta_P = 0.13\,\mu$m; $\varphi_0^P = 50$ fJ.

In order to visualise the resulting 3D SF distributions, two output variables are considered. Firstly, we utilise the average SF activation level $\overline{\eta}$ at each integration point, given as

$$\overline{\eta} = \sum_{k=1}^{n} \frac{\eta_k}{n} \tag{16}$$

where n is the total number (240) of discrete fibre orientations at each point. Secondly, in order to identify regions of the cell cytoplasm in which SFs are aligned in a dominant direction, a circular variance is defined to quantify the difference between the most highly activated fibre, $\eta_{\max}$, and the average fibre activation, $\overline{\eta}$, at each integration point. The circular variance Π is defined as:

$$\Pi = \eta_{\max} - \overline{\eta} \tag{17}$$

This variable simply reflects the degree of stress fibre bundling in a dominant direction at any point in the cytoplasm. In order to quantify the results on a whole-cell level, volume-averaged and area-averaged quantities are calculated by summing the quantity over the cell volume and area respectively:

$$X^* = \frac{1}{V}\int_V X \, \mathrm{d}V \qquad X^\dagger = \frac{1}{A}\int_A X \, \mathrm{d}A \tag{18}$$

where X is the quantity in question and V and A are the total volume of the relevant volume or area, where area is defined as the segment of the cell membrane adhering to the substrate.

3 Results

3.1 Increasing substrate stiffness increases SF and FA formation

The predicted distribution of SFs in cells adhered to elastic substrates is presented in Fig. 3a. The contour plots show the average level of SF formation at each point in the cell on substrates with moduli of 0.2–20,000 kPa. Supplementary Figure S1 shows the location of the dominant SFs, i.e., the SF circular variance (Π). The results show the steady-state distribution following 800 s of signal driven SF growth. The average SF formation is computed to be highest in cells simulated on the stiffest substrate. SFs are predicted to form near the base of the cell at the adhesion to the substrate. In order to quantify the differences in SF formation, volume-averaged values of SF formation and SF circular variance are calculated for the entire cytoplasm, as shown in Fig. 3b,c. Both the average SF and circular variance increase between 0.1 and 100 kPa, at which point a plateau is reached, and no further increase in SF formation is computed.

The stiffer substrates provide more support for SF tension, which leads to less fibre dissociation, as predicted by Eq. 3. The activation level of the most highly activated fibre at a given point in the cell, $\eta_{\max}$, is higher, causing increased SF formation. It should be noted that although the average SF formation, $\overline{\eta}$, is generally higher on stiffer substrates, the maximum fibre activation shows a greater increase, and therefore, a higher circular variance ($\Pi = \eta_{\max} - \overline{\eta}$) is computed on stiffer substrates.

The concentration of FA binding integrins on the cell surface is shown in Fig. 4a for cells adhered to a range of different substrates. The dimensionless concentration of bound, high affinity integrins (ξ_H/ξ_0) is shown as a function of the dimensionless radial coordinate. The area-averaged FA concentration is computed for each cell and presented as a function of substrate stiffness in Fig. 4b. Higher FA concentrations are computed for cells adhered to stiffer substrates, as expected due to tension from the higher levels of SF formation described above. FA concentrations are higher near the cell periphery for all substrates, and on the stiffer substrates (>200 kPa), a small area of FAs are predicted to form beneath the nucleus.

3.2 Substrate stiffness alters cell shape, nucleus stresses, and cellular tractions

In Fig. 5a, the effect of substrate stiffness on steady-state cell height is shown. On compliant substrates (<2 kPa), the cell height is 6.7 μm, and on stiffer substrates (>100 kPa), the height is 5.3 μm. The height of the cell before the introduction of cellular contractility is shown as a dashed line (7.5 μm). The average stress in the nucleus is computed to increase from 70 Pa on compliant substrates to 600 Pa on stiffer substrates, as shown in Fig. 5b. The stress in the nucleus increases between 1 and 100 kPa; however, outside of this range substrate stiffness does not significantly alter the stress. The increased SF formation seen on stiffer substrates generates more tension in the cell, which causes the computed increase in nucleus stress and decrease in cell height. The computed

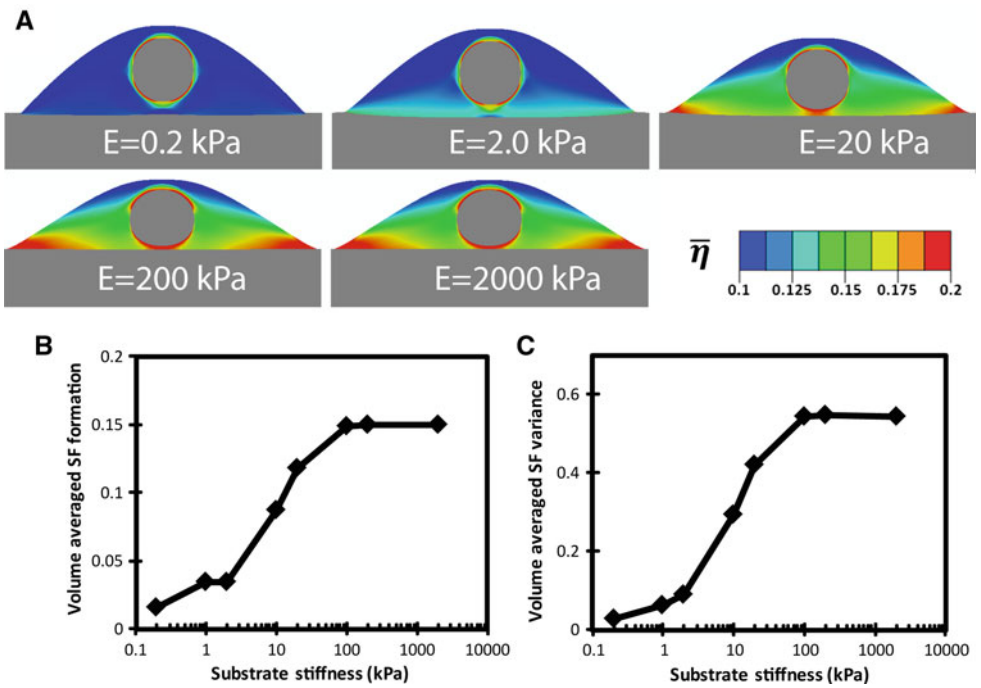

Fig. 3 Contour plot of average stress fibre (SF) formation for cells seeded on elastic substrates (**a**). The average SF activation level is summed over the volume of the cytoplasm (**b**), and circular variance of SF formation (max–average) at each point is summed over the volume of the cytoplasm (**c**); both are shown as a function of substrate stiffness

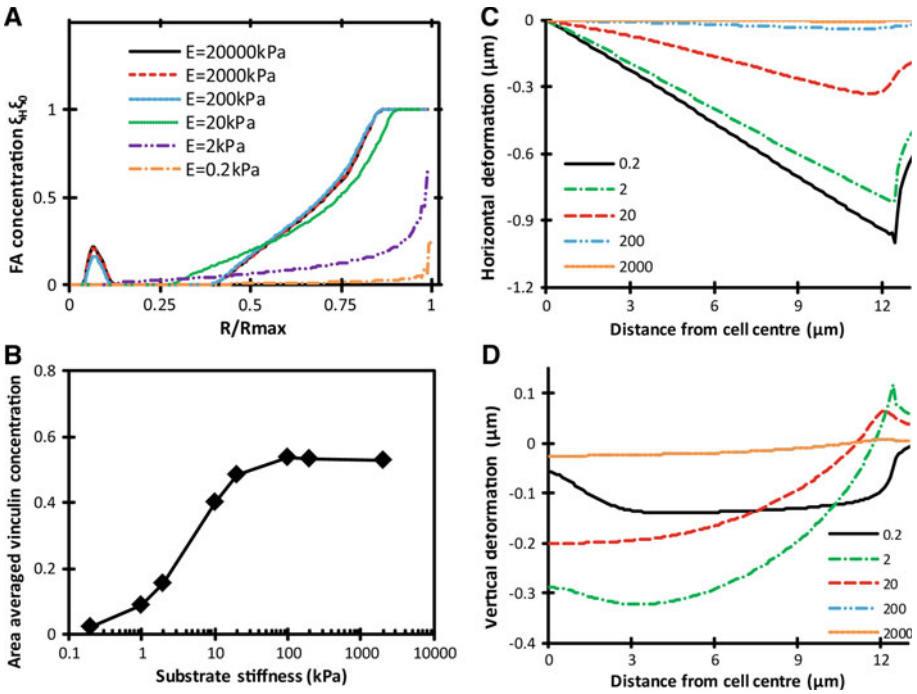

Fig. 4 Predicted concentration of focal adhesion (FA) integrins as a function of distance from cell centre for cells seeded on elastic substrates (**a**). Surface-averaged FA concentration for each cell is shown as a function of substrate stiffness (**b**). The deformation of the substrate due to the contractile action of the cell is shown in **c**, **d** for each substrate stiffness

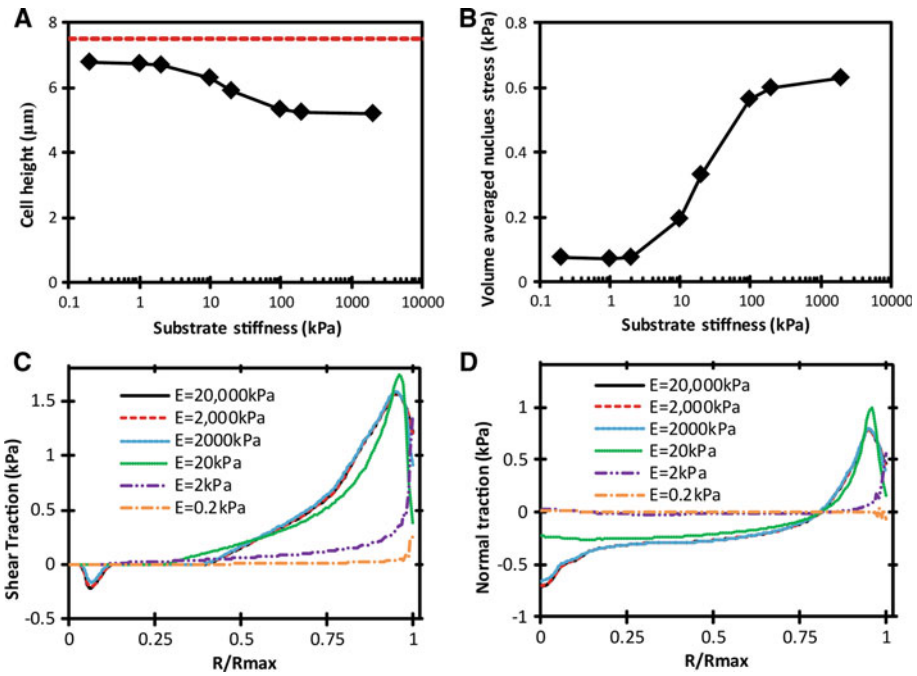

Fig. 5 Cell height (**a**) and averaged nucleus stress (**b**) as a function of substrate stiffness. Surface shear tractions (**c**) and normal tractions (**d**) as a function of distance from cell centre for cells on elastic substrates

shear traction exerted on the substrate by the cell is shown in Fig. 5c as a function of the dimensionless radial coordinate. As expected, higher shear tractions are predicted for stiffer substrates, and for each cell, the tractions are highest near the cell periphery. Tractions in the normal direction are shown in Fig. 5d, with positive tractions only at the cell periphery. The negative normal tractions indicate that the cell is compressed into the substrate in the central region. Cell deformations are shown in Fig. 4c,d for cells adhered to a range of substrates. Horizontal deformations in the plane of the substrate due to the contractile action of the cell are predicted to increase as substrate compliance decreases. The largest horizontal displacements are at the cell periphery, where FA concentrations are predicted to be highest. The predicted vertical deformations show that the cell creates a crater-like indentation in the substrate, with positive or upwards deformations at the cell periphery and a depression, or downwards deformation, at the interior of the cell. It should be noted that the deepest inden-

tation and highest ridge are both computed for the substrate with a stiffness of 2 kPa, which is not the most compliant substrate. On substrates more compliant than 2 kPa, SF formation is not sufficient to cause large deformations of the substrate.

3.3 Cellular contractility and substrate stiffness

The effect of cellular contractility on the substrate-dependent response of cells is shown in Fig. 6. The SF circular variance for each cell is shown for contractility levels representing smooth muscle cells, fibroblasts, and chondrocytes. Fig. 6a shows that the SF circular variance is decreased on more compliant substrates for all cell types. On very stiff substrates, the circular variance increases with increasing contractility; however, on very compliant substrates, the circular variance decreases with increasing contractility. The SF circular variance, normalized by the maximum circular variance for each cell type, is shown in Fig. 6b. This normalised plot shows that the relative change in circular variance is greatest for more contractile cells. Lower substrate stiffness causes a decrease in both the average and maximum SF formation; however, a smaller decrease of average SF formation is predicted for less contractile cells causing the trends in Fig. 6a,b. It should also be noted that in Fig. 6b, the range of substrate stiffness that causes the greatest change in the circular variance is lower for less contractile cells. Chondrocytes are predicted to be most sensitive on substrates more compliant than 2 kPa. In contrast, smooth muscle cells are predicted to be most sensitive in the range 1–100 kPa and fibroblasts in the range 0.1–10 kPa.

The nucleus stress computed for different cell types seeded on elastic substrates is shown in Fig. 6c. For all elastic substrates, decreasing contractility reduced the average nucleus stress. As was observed for the SF circular variance, two plateau regions were computed for very stiff and very compliant substrates in which the nucleus stress did not change significantly. Each cell type underwent the same relative change in nucleus stress, and highly contractile cells were more sensitive to stiffer substrates, as shown in the normalised plot in Fig. 6d.

3.4 Cell shape and substrate stiffness

The effect of cell shape on the cellular response to substrate stiffness is shown in Fig. 7. SF and FA formation is simulated in a spread cell with a round morphology, in addition to the spread cell simulated previously Fig. 7a. For SMCs, there is increase in the volume-averaged SF formation in the rounder cell compared to the highly spread cell for very compliant substrates Fig. 7b. For chondrocytes, the rounder cell shows significantly less sensitivity to substrate stiffness, with a bigger increase in the volume-averaged SF formation in the rounder cell for compliant substrates than that was observed for SMCs.

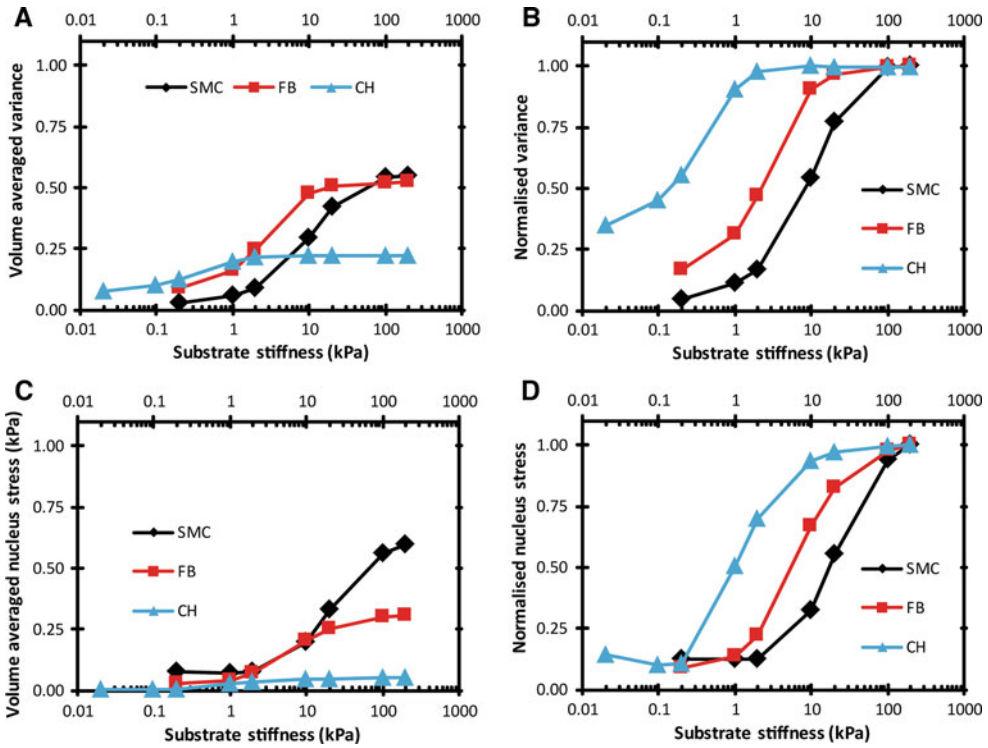

Fig. 6 Stress fibre (SF) circular variance averaged over the cytoplasm volume (**a**) and volume-averaged nucleus stress (**c**) as a function of substrate stiffness. The plots **a**, **c** are reproduced in **b**, **d**, normalized by the maximum value on the stiffest substrate to show relative changes on softer substrates

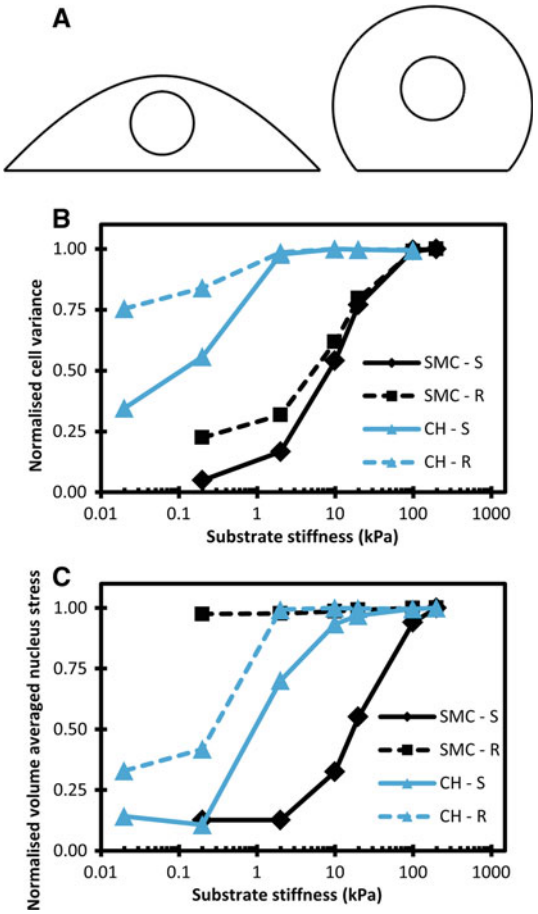

Fig. 7 **a** Original spread configuration (*left*) compared to modified round cell geometry (*right*). **b** Normalised stress fibre (SF) circular variance averaged over the cytoplasm volume (**b**) and normalised volume-averaged nucleus stress (**c**) as a function of substrate stiffness. *Note* values are normalized by the maximum value on the stiffest substrate to show relative changes on softer substrates. Data for the original spread geometry are shown with a solid line and data for the modified round geometry are shown with a dashed line

Interestingly, the average stress in the nucleus in round SMCs was not dependent on the substrate stiffness. As the nucleus in the round SMC is further away from the base of the cell, and hence further from the majority of SFs, the stress in the nucleus is not strongly influenced by changes in SFs near the base. In contrast, the SFs in the chondrocyte are not as dominant at the base of the cell; hence, changes in substrate stiffness lead to changes in SFs closer to the nucleus and consequently lead to changes in nucleus stress. It is important to note that Fig. 7c shows relative changes in nucleus stress and not absolute values.

3.5 Cells spreading on rigid substrates

Figure 8a–e shows the evolution of the cytoskeleton during spreading in a cell that is initially unattached from a rigid substrate. SF formation and cell spreading are driven by a constant signal over 1,400 s. The mixed mode interface model pulls the cell towards the surface, and the formation of FAs prevents lateral shortening of the cell. As the cell spreads, SFs are predicted to form at the periphery of the cell-substrate adhesion where FAs have been formed. Further spreading leads to SF formation in a band extending from the edge of the cell-substrate contact over the top of the nucleus. The combined active and passive interface model provides support for fibre tension, causing the distinct bands to emerge as the contact area between the cell and the substrate grows radially. Figure 8f shows the location of the FAs near the cell periphery at the end of the dominant band of fibres.

Figure 9 shows SF formation in cells simulated spreading on a rigid substrate using different contact formulations after ~240 s of spreading. In addition to the active and passive mixed mode formulation presented above and shown in Fig. 9a, cells are simulated using a completely passive model with a uniform distribution of adhesions and a linear spring model that does not allow for the sliding of integrins on the surface, as shown in Fig. 9a. In contrast to the mixed mode sliding model, the uniform distribution model does not provide enough tension for SF persistence, and reduced levels of SF formation are predicted. The integrins in the simplified model are stretched past the peak length, after which the force in the bond drops. This leads to a reduction in the interface stiffness, and hence, SFs dissociate following the reduction in tension. Finally, cells are simulated using a formulation that only considers the passive normal tractions, as shown in Fig. 9c. Due to the absence of FAs providing support for fibre tension, SFs parallel to the substrate shorten and hence dissociate near the base of the cell. Consequently, no SFs are predicted at the cell base, and the band of SFs extending from the periphery to the top of the nucleus is diminished in comparison with that computed with the active FA formation. Additionally, when SF tension is not supported by FAs, the cell contracts laterally and a significantly smaller contact area is computed (674 μm^2 compared to 857 μm^2). Furthermore, in the absence of non-specific tractions, SFs do not form near the base of the cell and the cell does not spread on the substrate, as shown in supplementary Figure S2.

The orientation of SFs following 550 s of cell spreading is shown in Figure 10 and in Movie S3. The vectors show the orientation of most dominant fibre at each point in the cell. Fibres at the base of the cell, particularly at the cell periphery, are predicted to form dominant bundles in the circumferential or hoop direction. In contrast, fibres in the dominant band of fibres leading from the cell periphery over the top of the cell and towards the nucleus are predicted to be aligned in the axisymmetric plane and are oriented in an approximately radial direction.

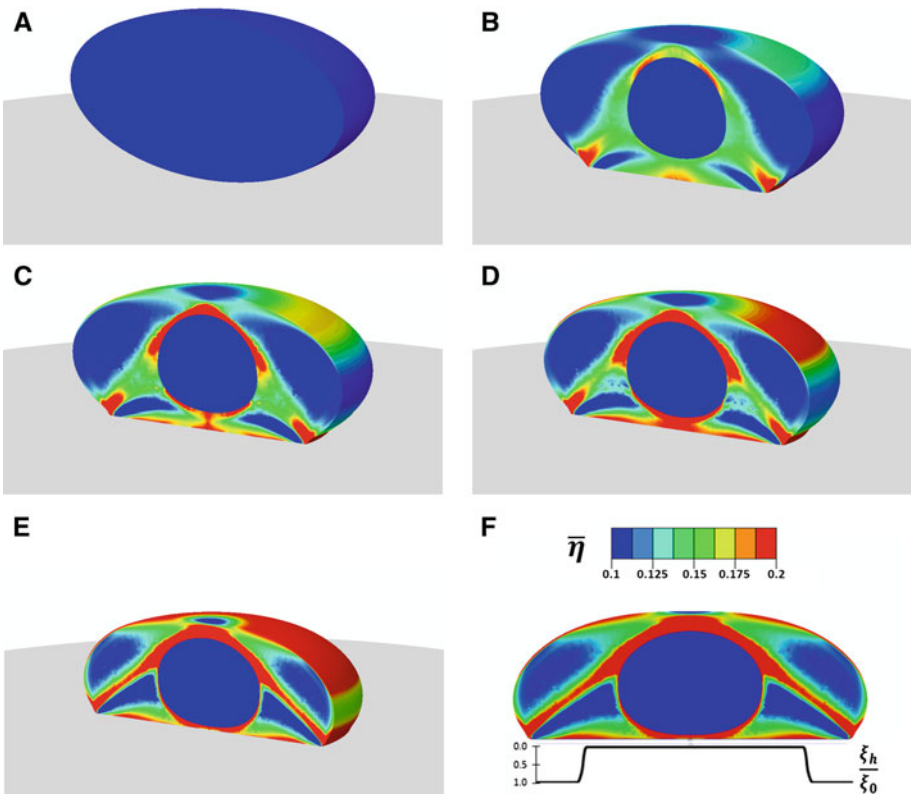

Fig. 8 Stress fibres evolution during cell spreading at 50, 150, 300, 400, and 550 s for a cell which is initially not in contact with a rigid substrate (**a**–**e**). The concentration of focal adhesion integrins is also shown (**f**)

4 Discussion

The current study presents a computational investigation of mutually dependent stress fibre (SF) and focal adhesion (FA) formation on elastic substrates in a 3D framework. Tension-dependent SF remodelling results in changes in the interface traction between the cell and substrate, which consequently lead to traction-dependent FA formation. Simulations reveal that SF contractility plays a critical role in the substrate-dependent response of cells. Compliant substrates do not provide enough tension for SF persistence, causing dissociation of SFs and lower FA formation. In contrast, cells on stiffer substrates are predicted to contain large amounts of dominant SFs, with FAs forming near the cell periphery at the end of the SF bundles. A transitional range of substrate stiffness is identified over which substrate stiffness effected the most significant changes in SF and FA formation, nucleus stress, and cell height. Outside of this transitional range substrate elasticity has a less significant effect on cell behaviour. Furthermore, different levels of cellular contractility representative of different cell phenotypes are found to alter this stiffness range. It should be noted that, for a given cell type, the substrate-dependent response is investigated using an unchanged parameter set. Finally, the spreading of a cell initially not in contact with a substrate is simulated. SF and FA formation evolves as the cell spread and leads to the formation of bands of SFs leading from the cell periphery over the nucleus. Inhibiting the formation of FAs during cell spreading is found to limit SF formation.

In the current study, more SFs and FAs are predicted to form in cells adhered to stiffer substrates. Simulations reveal that SFs form near the base of the cells, particularly at the cell periphery. Higher levels of bound FA integrins are computed in cells with a large amount of SFs. The inter-dependence of FAs and SFs is further shown on compliant substrates where low levels of SFs are accompanied by significantly smaller FAs. This trend has been widely observed experimentally for a range of cell types including endothelial (Byfield et al. 2009), mesenchymal stem cells (Engler et al. 2006), fibroblasts (Solon et al. 2007), and chondrocytes (Schuh et al. 2010). Experimental studies have attempted to quantify the changes in SF formation for cells seeded on elastic substrates: Byfield et al. (2009) report a doubling of the average SF fluorescence in endothelial cells on a 9 kPa substrate compared to 1.7 kPa. Solon et al. (2007) use densitometric quantification of Western blots to report a ∼50-fold increase in sedimented actin for fibroblasts seeded on a 15.2 kPa substrate compared to 0.7 kPa. Engler et al. (2006) show a linear increase in non-muscle myosin fluorescence in mesenchymal stem cells on elastic substrates ranging from 0.1 to 10 kPa. The experimental quantifications of Engler et al. (2006) and Solon et al. (2007) are reproduced and superimposed on the levels of SF actin formation predicted in the current study, as shown in Fig. 12. Furthermore, SFs are reported to form distinct

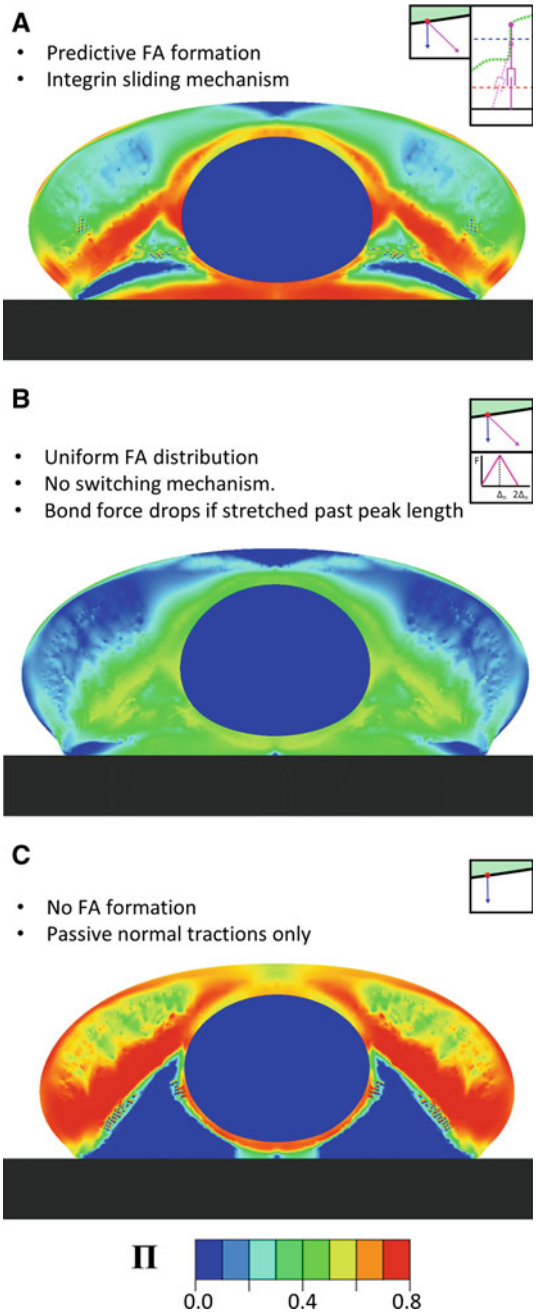

Fig. 9 Stress fibre (SF) formation for a cell simulated with an active mixed mode formulation (**a**); for a cell with a uniform distribution of focal adhesions (FA) and no mechanism to allow for the sliding of integrins along ligands (**b**); and for a cell simulated with a passive interface model that acts only in the normal direction (**c**). SFs are shown after 240 s

bundles on stiffer substrates, in contrast to more compliant substrates where stains for actin appear smeared (Engler et al. 2006; Yeung et al. 2005). Increased levels of FA formation are also reported for cells on stiffer substrates (Engler et al. 2006). These changes have been quantified experimentally by counting the number of distinct adhesions (Ren et al. 2008) or by calculating the total area of FAs on the cell surface (Goffin et al. 2006). Elineni and Gallant (2011) measured the intensity of FA integrins for cells adhered to circular adhesive patches, observing a significant peak of high affinity integrins at the cell periphery and a uniformly low level in the interior of the adhered area, which is in strong agreement with the distributions predicted here. For comparison, the results of Fig. 4 are superimposed upon the experimental data of Elineni and Gallant (2011) for axisymmetric fibroblasts adhered to circular micropatterned islands, as shown in Fig. 11. In both the simulated and experimental results, FAs are seen to form near the centre of the cell contact area; however, these FAs are only predicted to form near the nucleus for stiffer substrates. While experimental images predominantly show FA's at the cell periphery, experimental images of vinculin show smaller amounts of FA formation near the interior of the cell (Elineni and Gallant 2011). Experimental observations by Goffin et al. show FAs in a ring surrounding the nucleus; however, such FAs are not widely reported. The predicted level of FA formation under the nucleus is quiet low; therefore, such low levels of FA formation may not always be clearly visible.

The role of contractility was investigated in the current study by considering three cell phenotypes representing a spectrum of cellular contractility: smooth muscle cells, fibroblasts, and chondrocytes (in order of decreasing contractility). The parameters required to simulate the active contractility of these cells were identified in previous implementations of the material formulation employed here (Dowling et al. 2012; McGarry et al. 2009). The range of substrate stiffness that has the greatest effect on the substrate-dependent response of each cell type is identified by considering the level of SF formation and average nucleus stress. Simulations reveal that highly contractile SMCs are most sensitive over the range 1–100 kPa. In contrast, less contractile fibroblasts are sensitive over 0.1–10 kPa, and chondrocytes are most sensitive on substrates with a modulus less than 2 kPa. This link between substrate elasticity and the cellular contractility is supported by experimental observations. Ren et al. (2008) report that highly contractile myoblasts form well-defined FAs and numerous highly organised SF bundles on substrates stiffer than 300 kPa and also note significant changes in cell morphology over the range 100–300 kPa. In contrast, less contractile cells, such as chondrocytes, are reported to be sensitive to much more compliant ranges: substrates stiffer than 4 kPa are reported to lead to flattened morphologies, while less stiff substrates lead to rounded chondrocyte morphologies (Schuh et al. 2010; Subramanian and Lin 2005). SF circular variance is predicted to increase with increasing substrate stiffness. Therefore, cells are computed to form bundles that are more dominant on stiff substrates. Experimental observations of cells on different substrates show highly aligned SFs on stiff substrates, and in contrast, compliant substrates lead to less organised SF distributions(Discher and

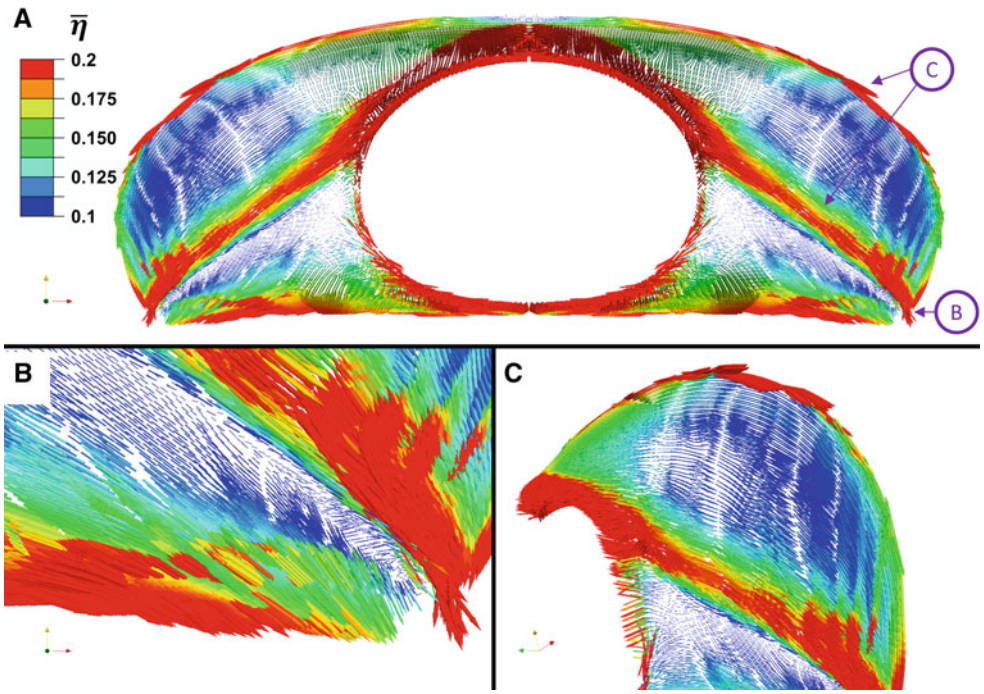

Fig. 10 The orientation of the most highly activated or dominant fibre is shown as a vector plot (**a**) with zoomed in views to highlight fibres oriented in the hoop direction at the base of the cell and at the cell periphery (**b**) and to highlight 2 bands of fibres leading radially from the cell periphery towards the nucleus and along the cortical area of the cell (**c**). The vector length represents the activation level of the dominant fibre, and the colour represents the average level of SF formation in all directions at each point

Janmey 2005). The predictions presented in the current study, which are strongly aligned with these experimental observations, suggest a strong link between the contractility of cells and the range of substrate stiffness over which they exhibit the greatest changes. In our framework, the contractile stress fibres are in mechanical equilibrium with the FA interface tractions and hence with stresses in the substrate; therefore, the inter-dependence of FA and stress fibres emerges without any assumptions regarding SF or FA distributions. Our coupled SF and FA framework offers a unique insight into the role of SF contractility and tension-dependent remodelling in the ability of cells to actively respond to substrate stiffness.

The current study predicts that the level of stress in the nucleus is affected by cellular contractility, substrate stiffness, and cell shape. Previous experimental studies have established the mechanical link between the cytoskeleton and the nucleus (Buxboim et al. 2010), and, in particular, that the removal of nuclear lamins also leads to disruption of the cytoskeleton (Broers et al. 2004). In the current study, the nucleus and the cytoplasm are simulated as two separate but continuous regions and it is important to note that no movement is permitted between the cytoplasm and the nucleus. While nuclear binding proteins are not explicitly included in the computational framework, the constraints at the cytoplasm–nucleus interface represent a uniform distribution of rigid nesprins. Significant differences have been reported in nuclear stresses and apparent stiffness levels between stem cells and differentiated phenotypes (Pajerowski et al. 2007). Furthermore, it is well established that substrate stiffness directs stem cell linage (Discher and Janmey 2005). Compliant substrates are reported to be neurogenic, while stiffer substrates are found to be myogenic, and comparatively, rigid substrates are osteogenic (Engler et al. 2006). The current study predicts substrate-dependent changes in nucleus stress for a given cell type using an

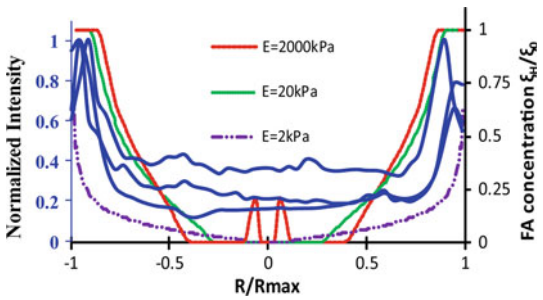

Fig. 11 Comparison of experimental observations of focal adhesion (FA) proteins for fibroblasts cells seeded on circular adhesive patches (shown as *solid blue lines*) and computational predictions of cells seeded on elastic substrates (for 2,000 kPa (*red*) 20 kPa (*green*) and 2kPa (*magenta*). Experimental data adapted from (Elineni and Gallant 2011) for three fibroblast cells adhered to a ~2,000 kPa substrate

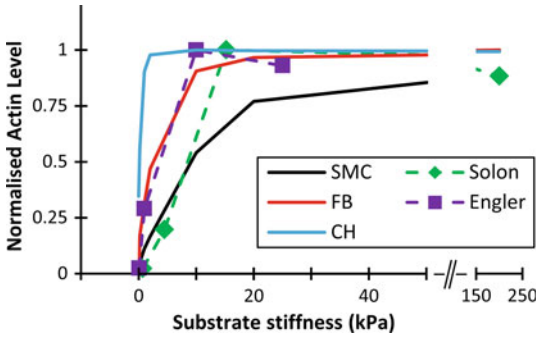

Fig. 12 Comparison of experimentally observed levels of SF actin formation (*dashed lines*) with predicted results (*solid lines*) as a function of substrate stiffness. Predicted results are shown for smooth muscle cells (SMCs), fibroblasts (FBs), and chondrocytes (CH). Experimental data are adopted from Engler et al. (2006) and Solon et al. (2007)

unchanged parameter set. Changes in both substrate stiffness and cell morphology are found to alter significantly the stress in the nucleus. In future experimental studies of substrate-dependent contractility, it would be interesting to restrict the spread area of the cell by micropatterning of the substrate and subsequently measuring the deformed configuration of the nucleus. Such an investigation may validate our prediction regarding cell shape and nucleus stress. The ability to accurately simulate nucleus stress offers a unique insight into the mechanical regulation of stem cell differentiation and will potentially provide a powerful predictive tool for tissue engineering applications.

The current study predicts the traction stress exerted by a cell on an elastic substrate and the resulting substrate deformations. The substrate deformations shown previously in Fig. 4c, d are reproduced as a contour plot and compared to the measurements of Hur et al. (2009) in Fig. 13. Computed substrate deformations are strongly supported by the 3D measurements of Hur et al. (2009), with both experimental and predicted deformations forming a crater-like shape with a depression (approximately 0.4 μm deep) at the centre of the cell surrounded by a ridge. Simulations also predict that shear tractions are highest at the cell periphery and highly dependent on substrate elasticity. On compliant substrates, shear tractions are computed to be ∼100 Pa in the interior of a smooth muscle cell, rising to 250 Pa at the cell periphery, whereas on stiffer substrates, tractions in the interior range up to 800 Pa rising to over 1.5 kPa at the periphery. Previous experimental studies have measured the surface shear tractions exerted by a cell using microbeads embedded in elastic gels (traction force microscopy) to calculate the deformation of the gel and hence determine the traction field (Wang et al. 2002). Tractions near the interior of the cell are typically 4–5 times lower than peak tractions at the cell periphery, with peaks of over 900 kPa reported for smooth muscle cells, dropping to 400 Pa halfway from the periphery to 200 Pa at the interior (Wang et al. 2002). Lower tractions are reported for less contractile epithelial cells with ∼50 Pa internally and 150–200 Pa at the cell periphery (Gavara et al. 2006; Roca-Cusachs et al. 2008). The tractions predicted

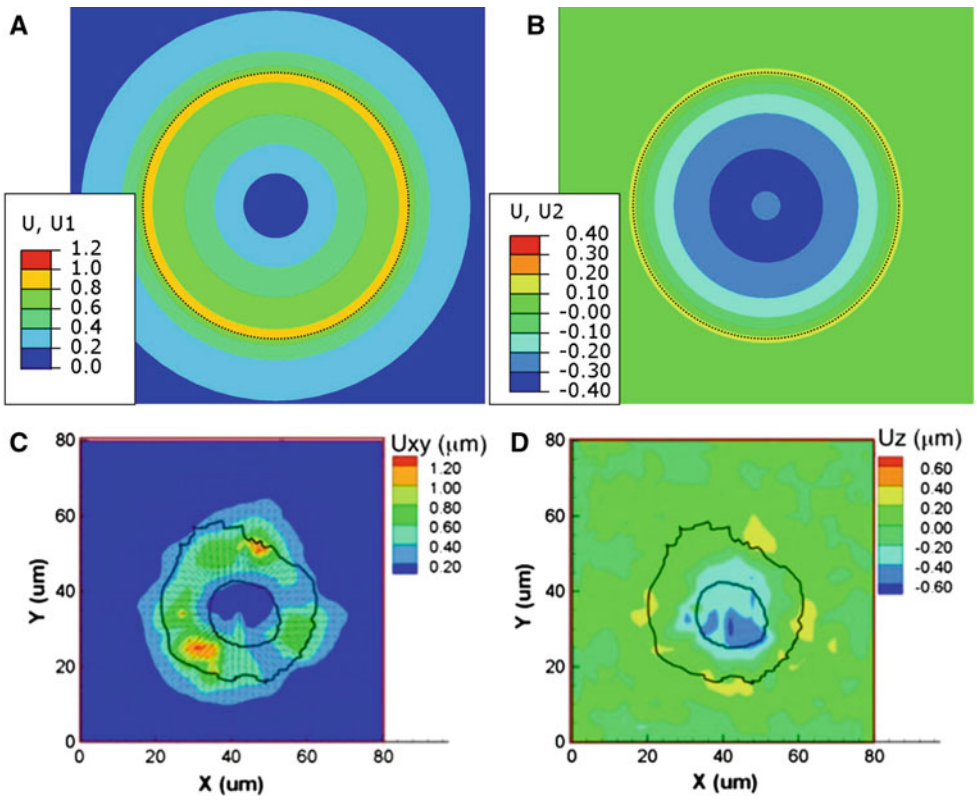

Fig. 13 Computed horizontal (**a**) and vertical (**b**) deformations for fibroblasts adhered to a 2 kPa substrate. Experimentally observed deformations (**c**,**d**) for an endothelial cell adhered to a 3.78 kPa substrate (adopted from Hur et al. (2009)). The cell outline is shown as a *black line* in each image

in the current study are strongly aligned with such experimental data. Furthermore, experimental studies have also reported that substrate stiffness influences cellular tractions; tractions for endothelial cells seeded on a 1 kPa substrate are reported to be ∼200 Pa, whereas significantly higher tractions of ∼1,000 Pa are measured for endothelial cells on 5 or 10 kPa substrates (Califano and Reinhart-King 2010). A similar dependence of shear tractions on substrate stiffness is predicted by the modelling framework used in the current study. It should be noted that, in the present study, significant tractions in the normal direction are computed for cells on stiffer substrates. Experimental techniques, such as traction force microscopy, typically measure only the shear component. However, both normal and shear tractions can lead to stretching of FA bonds. Considering only the shear component of the contact tractions may lead to underestimation of the forces exerted on FA integrins at the periphery of cells on very stiff substrates.

The latter part of the current study presents simulations of a cell attaching to and spreading on a rigid substrate. The mixed mode FA model and passive tractions promote the spreading and flattening of the cell, while resisting the lateral contraction of the cell due to SF contractility. During cell spreading, the actin cytoskeleton evolves as the size of the adhered surface grows. FAs are predicted to form at the cell periphery and support fibre tension leading to the formation of a band of SFs from the cell periphery over the nucleus. Such long SFs that extend from the cell periphery over the nucleus have been observed experimentally (Goffin et al. 2006; Elineni and Gallant 2011). The importance of including mixed mode FA behaviour is demonstrated by simulating cell spreading without these essential biophysical processes. Simulations reveal a uniform distribution of adhesions without a mechanism that allows for the sliding of integrins along the substrate results in reduced levels of SF formation. The simplified adhesion model does not provide the required support for SF tension, and significantly, lower levels of fibre formation are predicted. Furthermore, using a formulation that only considers the normal passive tractions leads to an unrealistic distribution of SFs. The 3D framework predicts the orientation of SFs as the cell spreads, and dominant bundles of SFs are identified in the circumferential direction at the cell periphery and in the radial direction leading towards the cell nucleus. In experimental observations where the cell has formed an approximately axisymmetric geometry, similar to that simulated here, the predicted orientations are found to be in agreement with experimentally observed dominant fibre bundles (Oakes et al. 2012; Potter et al. 1998).

While the current study represents a step forward in the computational investigation of SF and FA behaviour of cells spread on elastic substrates, a number of limitations exist that should be considered in future studies. Experimental studies have shown that protrusion forces exerted by filopodia and lamellipodia during spreading can be ∼5 and ∼20 pN (Cojoc et al. 2007). These phenomena have not been considered in the current study; however, future computational studies of cell spreading should consider these processes. By incorporating the behaviour of actin protrusions, it is likely that the simulations of cell spreading will predict a flatter cell morphology. A limitation of the current study is that the predicted spread cell bulges outwards at the cell periphery; such bulging is not consistent with experimental observations of in-vitro spread cells. Previous experimental studies have also shown that microtubules undergo complex deformations that merit investigation the in future studies (Brangwynne et al. 2006); however, microtubules and other components of the cell have all been included in the current formulation as part of a passive hyperelastic component.

A recent experimental/computational study by Tondon et al. (2012) used asymmetric stretch waveforms during cyclic stretch, and cell lengthening rate was found to influence SF dissociation more than cell shortening rate. Alignment of stress fibres is observed for high strain rate loading and not for low strain rate loading. The kinetic equation implemented used in the current study would not capture this result if cell alignment is entirely a function of unloading strain rate. However, loading strain rates may influence cell signalling, stress fibre formation, and focal adhesion rupture under dynamic conditions. A full investigation of the ability of our modelling framework to capture the results of Tondon et al. (2012) under dynamic boundary conditions should be performed in a separate study. Such a study may result in further model development including physiological signalling in response to cyclic stretching and altered stress fibre behaviour under high lengthening rates. In the current study, the cell is not subjected to externally applied loads, and the rate of deformation due to SF contractility is sufficiently slow such that the tri-linear model may be used.

Cellular signalling drives SF remodelling, and the exponentially decaying signal in the current study is based on the observations of Roberts et al. (2001) and Ruwhof et al. (2001). In these studies, an approximately exponentially decaying calcium signal is detected following mechanical loading. While calcium signalling regulates SF contractility in SMCs (Somlyo and Somlyo 1994), other signalling pathways may be more relevant in other cell types. In the material model presented here, the kinetics of the signalling pathway and the proteins involved are not specifically considered. Instead, a simplified spatially uniform signal is used to represent all signalling pathways inclusive of proteins such as Rho-GTPases, Rac and Rho when they are involved. A complete biochemical analysis of the complex signalling pathways involved in the formation of stress fibres is beyond the scope of the current study (see Zeng et al. 2011; Pollard et al. 2000). In the latter part of the present study, a

continuous signal is used to represent the sustained signalling from stretch-activated channels. A recent mechanosensitive intracellular signalling formulation incorporates a feedback loop between SF contractility, FA tractions, and signalling pathways (Pathak et al. 2011); however, this mechanism has not been implemented in a 3D framework. Future studies should incorporate such a signalling feedback to avoid the assumptions of constant or decaying signals used here.

In the current study, different categories of stress fibres have not been considered. In the previous study by Hotulainen and Lappalainen (2006), it is noted that transverse arcs can form between two dorsal SFs, and as the transverse arc contracts, form a ventral SF. While the origins of these fibres maybe different, the underlying myosin-driven contractility is similar; therefore, a unified model can be justified as a first step. The contractile nature of these transverse arcs is confirmed by Hotulainen & Lappalainen by inhibiting myosin ATPase activity by treating cells with blebbistatin, which resulted in a complete loss of transverse arcs in the cell. Naumanen et al. (2008) describe transverse arcs as α-actinin-decorated actin filaments and that these actin filament structures assemble endwise with myosin bundles to form contractile transverse arcs. For cells similar to those of Naumanen et al. (U2OS), Oakes et al. (2012) report that transverse arcs generate large amounts of tension that is relayed to FAs via dorsal SFs. Transverse arcs have been shown to be involved in cell migration (Gardel et al. 2010), and the role of actin contractility has been investigated recently by the computational study of Shemesh et al. (2012).

Axially symmetric finite element models used in the current study are based on experimental observations of spread cell morphologies (Caille et al. 2002; Thoumine et al. 1999). Axial symmetry has been successfully used in previous computational studies to minimize computational cost (Caille et al. 2002; Nguyen et al. 2010; Ofek et al. 2009; Haider and Guilak 2002; Rowat et al. 2005). A previous 3D investigation of the role of SF contractility in the compression resistance of cells,which used the material model employed in the current study, reported similar trends for axisymmetric and polarised cell geometries (Ronan et al. 2012).

The tensegrity model (Ingber 1993) has been used to investigate the response of contractile cells to substrate elasticity (Santis et al. 2011). This study also identifies the substrate stiffness over which the cell shows the greatest sensitivity to substrate elasticity. However, the tensegrity model requires a-priori knowledge of the SF distribution in the cell, and experimental investigation has shown that the disruption of microtubules results in an increase in the traction force generated by cells (Kolodney and Elson 1995), suggesting that the strut-based structure of the tensegrity model overlooks other essential biomechanical elements of the cell. The model of Novak et al. (2004) incorporates a feedback loop between adhesion formation and the assembly of actin fibres. The inclusion of this feedback loop replicates two key phenomena: the arrangement of long stress fibres and the tendency for adhesions to form at the cell periphery. However, the model of Novak et al. assumes that stress fibres form randomly at adhesion sites in proportion to the size of the adhesion and dissociate at a constant rate. Mohrdieck et al. (2005) has developed a model for the actin cytoskeleton as a discrete set of fibres linking adhesion sites. However, this model assumes a predefined distribution of fibres which are subjected to a uniform prestrain and does not allow for changes in the cytoskeleton based on the underlying cell processes. Zeng and Li (2011) simulate cell spreading by considering the cytoplasm as a liquid crystal material that interacts with an elastic substrate via a potential-based attractive adhesive force. This model predicts different spread morphologies for cells on substrates with different stiffness. Ni and Chiang (2007) simulate changes in cell morphology across a range of substrate stiffness by minimizing the free energy of the cell and the cell-substrate interaction. This free energy model consists of a planar cell with a band of uniformly distributed adhesions at the cell edge. This approach identifies a range of substrate stiffness over which the cell forms a "branched" morphology. Olberding et al. (2010) consider the thermodynamic equilibrium of bound and unbound binding proteins in a manner similar to that of the current study. Interestingly, Olberding et al. explicitly consider the kinetics of the binding process, and consequently, a finite adhesion strength emerges from the binding kinetics without specifying a strength for individual bonds. Shemesh et al. (2012)) investigate the stick/slip behaviour between actin and focal adhesions during the self-organisation of the cytoskeleton at the cell front. In contrast, our model does not involve growth of the actin gel network but instead deals with the interaction between SFs and FAs via the equilibrium of internal contractile forces (due to SFs) with external tractions (reactions due to FAs). The contractility of the cytoskeleton is treated as a constant force or membrane tension in many of the above models, and therefore, their models are limited to analysing adhesion dynamics in the absence of broader interactions within the cell. In contrast, the framework presented in the current study is based on the key biomechanical cellular processes of SF and FA formation and evolution; this allows for further understanding of the traction based inter-dependence of SFs and FAs

5 Conclusions

In the current study, we have predicted the substrate-dependent response of contractile cells with no predefined SF or FA arrangement. Each cell phenotype is simulated using an unchanged set of parameters, predicting increased

levels of SF and FA formation on stiffer substrates. The predictions of this mutually dependent material-interface framework are strongly supported by experimental observations of cells adhered to elastic substrates. SF contractility is found to strongly influence the substrate-dependent response of cells, including changes in nuclear stress and cell tractions. This framework is also used to simulate cell spreading where an unadhered cell geometry is initially assumed. Again, spreading simulations highlight the importance of inter-dependent SF and FA formation.

Acknowledgments Funding support was provided by the Irish Research Council for Science, Engineering and Technology (IRCSET) postgraduate scholarship under the EMBARK initiative and by the Science Foundation Ireland Research Frontiers Programme (SFI-RFP/ENM1726). The authors acknowledge the SFI/ HEA Irish Centre for High-End Computing (ICHEC) for the provision of computational facilities and support.

References

Balaban NQ, Schwarz US, Riveline D, Goichberg P, Tzur G, Sabanay I, Mahalu D, Safran S, Bershadsky A, Addadi L, Geiger B (2001) Force and focal adhesion assembly: a close relationship studied using elastic micropatterned substrates. Nat Cell Biol 3(5):466–472. doi:10.1038/35074532

Bell G (1978) Models for the specific adhesion of cells to cells. Science 200(4342):618–627. doi:10.1126/science.347575

Brangwynne CP, MacKintosh FC, Kumar S, Geisse NA, Talbot J, Mahadevan L, Parker KK, Ingber DE, Weitz DA (2006) Microtubules can bear enhanced compressive loads in living cells because of lateral reinforcement. J Cell Biol 173(5):733–741. doi:10.1083/jcb.200601060

Broers JLV, Peeters EAG, Kuijpers HJH, Endert J, Bouten CVC, Oomens CWJ, Baaijens FPT, Ramaekers FCS (2004) Decreased mechanical stiffness in LMNA-/- cells is caused by defective nucleo-cytoskeletal integrity: implications for the development of laminopathies. Hum Mol Genet 13(21):2567–2580. doi:10.1093/hmg/ddh295

Bruinsma R (2005) Theory of force regulation by nascent adhesion sites. Biophys J 89(1):87–94

Burridge K, Fath K, Kelly T, Nuckolls G, Turner C (1988) Focal adhesions: transmembrane junctions between the extracellular matrix and the cytoskeleton. Ann Rev Cell Biol 4(1):487–525. doi:10.1146/annurev.cb.04.110188.002415

Buxboim A, Ivanovska IL, Discher DE (2010) Matrix elasticity, cytoskeletal forces and physics of the nucleus: how deeply do cells 'feel' outside and in? J Cell Sci 123(Pt 3):297–308. doi:10.1242/jcs.041186

Byfield FJ, Reen RK, Shentu TP, Levitan I, Gooch KJ (2009) Endothelial actin and cell stiffness is modulated by substrate stiffness in 2D and 3D. J Biomechan 42(8):1114–1119

Caille N, Thoumine O, Tardy Y, Meister J-J (2002) Contribution of the nucleus to the mechanical properties of endothelial cells. J Biomechan 35(2):177–187

Califano J, Reinhart-King C (2010) Substrate stiffness and cell area predict cellular traction stresses in single cells and cells in contact. Cell Mol Bioeng 3(1):68–75. doi:10.1007/s12195-010-0102-6

Cheng QH, Liu P, Gao HJ, Zhang YW (2009) A computational modeling for micropipette-manipulated cell detachment from a substrate mediated by receptor-ligand binding. J Mech Phys Solids 57(2):205–220. doi:10.1016/j.jmps.2008.11.003

Cojoc D, Difato F, Ferrari E, Shahapure RB, Laishram J, Righi M, Di Fabrizio EM, Torre V (2007) Properties of the force exerted by filopodia and lamellipodia and the involvement of cytoskeletal components. PLoS One 2(10):e1072. doi:10.1371/journal.pone.0001072

Danjo Y, Gipson IK (1998) Actin 'purse string' filaments are anchored by E-cadherin-mediated adherens junctions at the leading edge of the epithelial wound, providing coordinated cell movement. J Cell Sci 111(22):3323–3332

De Santis G, Lennon A, Boschetti F, Verhegghe B, Verdonck P, Prendergast P (2011) How can cells sense the elasticity of a substrate?: an analysis using a cell tensegrity model. Eur Cells Mater 22:202–213

Deshpande VS, McMeeking RM, Evans AG (2006) A bio-chemo-mechanical model for cell contractility. Proc Natl Acad Sci 103(38):14015–14020. doi:10.1073/pnas.0605837103

Deshpande VS, McMeeking RM, Evans AG (2007) A model for the contractility of the cytoskeleton including the effects of stress-fibre formation and dissociation. Proc Roy Soc A Math Phys Eng Sci 463(2079):787–815. doi:10.1098/rspa.2006.1793

Deshpande VS, Mrksich M, McMeeking RM, Evans AG (2008) A bio-mechanical model for coupling cell contractility with focal adhesion formation. J Mech Phys Solids 56(4):1484–1510

Discher DE, Janmey P (2005) Tissue cells feel and respond to the stiffness of their substrate. Science 310(5751):1139–1143. doi:10.1126/science.1116995

Dowling EP, Ronan W, Ofek G, Deshpande VS, Athanasiou KA, McMeeking RM, McGarry JP (2012) The effect of remodelling and contractility of the actin cytoskeleton on the shear resistance of single cells: a computational and experimental investigation. J Roy Soc Interf 9(77):3469–3479. doi:10.1098/rsif.2012.0428

Elineni KK, Gallant ND (2011) Regulation of cell adhesion strength by peripheral focal adhesion distribution. Biophys J 101(12):2903–2911

Engler AJ, Sen S, Sweeney HL, Discher DE (2006) Matrix elasticity directs stem cell lineage specification. Cell 126(4):677–689. doi:S0092-8674(06)00961-5

Gardel ML, Schneider IC, Aratyn-Schaus Y, Waterman CM (2010) Mechanical integration of actin and adhesion dynamics in cell migration. Ann Rev Cell Dev Biol 26:315–333

Gavara N, Sunyer R, Roca-Cusachs P, Farré R, Rotger M, Navajas D (2006) Thrombin-induced contraction in alveolar epithelial cells probed by traction microscopy. J Appl Physiol 101(2):512–520. doi:10.1152/japplphysiol.00185.2006

Goffin JM, Pittet P, Csucs G, Lussi JW, Meister JJ, Hinz B (2006) Focal adhesion size controls tension-dependent recruitment of alpha-smooth muscle actin to stress fibers. J Cell Biol 172(2):259–268

Haider MA, Guilak F (2002) An axisymmetric boundary integral model for assessing elastic cell properties in the micropipette aspiration contact problem. J Biomech Eng 124(5):586–595

Hill AV (1938) The heat of shortening and the dynamic constants of muscle. Proc Roy Soc Lond Ser B Biol Sci 126(843):136–195. doi:10.1098/rspb.1938.0050

Hotulainen P, Lappalainen P (2006) Stress fibers are generated by two distinct actin assembly mechanisms in motile cells. J Cell Biol 173(3):383–394. doi:10.1083/jcb.200511093

Hur SS, Zhao Y, Li YS, Botvinick E, Chien S (2009) Live cells exert 3-dimensional traction forces on their substrata. Cell Mol Bioeng 2(3):425–436

Ingber DE (1993) Cellular tensegrity: defining new rules of biological design that govern the cytoskeleton. J Cell Sci 104:613–613

Isenberg BC, DiMilla PA, Walker M, Kim S, Wong JY (2009) Vascular smooth muscle cell durotaxis depends on substrate stiffness gradient strength. Biophys J 97(5):1313–1322. doi:10.1016/j.bpj.2009.06.021

Kaunas R, Hsu HJ (2009) A kinematic model of stretch-induced stress fiber turnover and reorientation. J Theor Biol 257(2):320–330. doi:10.1016/j.jtbi.2008.11.024

Kaunas R, Hsu HJ, Deguchi S (2011) Sarcomeric model of stretch-induced stress fiber reorganization. Cell Health Cytoskelet 3:13–22

Leckband D, Israelachvili J (2001) Intermolecular forces in biology. Quart Rev Biophys 34(02):105–267

Leckband D, Israelachvili J, Schmitt F, Knoll W (1992) Long-range attraction and molecular rearrangements in receptor-ligand interactions. Science (New York, NY) 255(5050):1419

Levental KR, Yu H, Kass L, Lakins JN, Egeblad M, Erler JT, Fong SFT, Csiszar K, Giaccia A, Weninger W, Yamauchi M, Gasser DL, Weaver VM (2009) Matrix crosslinking forces tumor progression by enhancing integrin signaling. Cell 139(5):891–906. doi:10.1016/j.cell.2009.10.027

Lo C-M, Wang H-B, Dembo M (2000) Cell movement is guided by the rigidity of the substrate. Biophys J 79(1):144–152. doi:10.1016/s0006-3495(00)76279-5

McGarry JP, Fu J, Yang MT, Chen CS, McMeeking RM, Evans AG, Deshpande VS (2009) Simulation of the contractile response of cells on an array of micro-posts. Philos Trans Roy Soc A Math Phys Eng Sci 367(1902):3477–3497

Mohrdieck C, Wanner A, Roos W, Roth A, Sackmann E, Spatz JP, Arzt E (2005) A theoretical description of elastic pillar substrates in biophysical experiments. Chemphyschem 6(8):1492–1498

Naumanen P, Lappalainen P, Hotulainen P (2008) Mechanisms of actin stress fibre assembly. J Microsc 231(3):446–454. doi:10.1111/j.1365-2818.2008.02057.x

Nguyen BV, Wang QG, Kuiper NJ, El Haj AJ, Thomas CR, Zhang Z (2010) Biomechanical properties of single chondrocytes and chondrons determined by micromanipulation and finite-element modelling. J Roy Soc Interf 7(53):1723–1733. doi:10.1098/rsif.2010.0207

Ni Y, Chiang MYM (2007) Cell morphology and migration linked to substrate rigidity. Soft Matter 3(10):1285–1292

Novak IL, Slepchenko BM, Mogilner A, Loew LM (2004) Cooperativity between cell contractility and adhesion. Phys Rev Lett 93(26):268109

Oakes PW, Beckham Y, Stricker J, Gardel ML (2012) Tension is required but not sufficient for focal adhesion maturation without a stress fiber template. J Cell Biol 196(3):363–374. doi:10.1083/jcb.201107042

Ofek G, Natoli RM, Athanasiou KA (2009) In situ mechanical properties of the chondrocyte cytoplasm and nucleus. J Biomech 42(7):873–877. doi:10.1016/j.jbiomech.2009.01.024

Olberding JE, Thouless MD, Arruda EM, Garikipati K (2010) The non-equilibrium thermodynamics and kinetics of focal adhesion dynamics. PLoS One 5(8):e12043

Pajerowski JD, Dahl KN, Zhong FL, Sammak PJ, Discher DE (2007) Physical plasticity of the nucleus in stem cell differentiation. Proc Natl Acad Sci USA 104(40):15619–15624. doi:10.1073/pnas.0702576104

Paszek MJ, Zahir N, Johnson KR, Lakins JN, Rozenberg GI, Gefen A, Reinhart-King CA, Margulies SS, Dembo M, Boettiger D, Hammer DA, Weaver VM (2005) Tensional homeostasis and the malignant phenotype. Cancer cell 8(3):241–254

Pathak A, Deshpande VS, Evans AG, McMeeking RM (2012) Simulations of Cell Behavior on Substrates of Variegated Stiffness and Architecture. In: Holzapfel GA, Kuhl E (eds) Computer Models in Biomechanics. From Nano to Macro. Springer, The Netherlands, pp 25–41.

Pathak A, Deshpande VS, McMeeking RM, Evans AG (2008) The simulation of stress fibre and focal adhesion development in cells on patterned substrates. J R Soc Interf 5(22):507–524

Pathak A, McMeeking RM, Evans AG, Deshpande VS (2011) An analysis of the cooperative mechano-sensitive feedback between intracellular signaling, focal adhesion development, and stress fiber contractility. J Appl Mech 78(4):041001

Pollard TD, Blanchoin L, Mullins RD (2000) Molecular mechanisms controlling actin filament dynamics in nonmuscle cells. Ann Rev Biophys Biomol Struct 29(1):545–576. doi:10.1146/annurev.biophys.29.1.545

Potter DA, Tirnauer JS, Janssen R, Croall DE, Hughes CN, Fiacco KA, Mier JW, Maki M, Herman IM (1998) Calpain regulates actin remodeling during cell spreading. J Cell Biol 141(3):647–662

Ren K, Crouzier T, Roy C, Picart C (2008) Polyelectrolyte multilayer films of controlled stiffness modulate myoblast cell differentiation. Adv Funct Mater 18(9):1378–1389. doi:10.1002/adfm.200701297

Roberts SR, Knight MM, Lee DA, Bader DL (2001) Mechanical compression influences intracellular Ca2+ signaling in chondrocytes seeded in agarose constructs. J Appl Physiol 90(4):1385–1391

Roca-Cusachs P, Alcaraz J, Sunyer R, Samitier J, Farré R, Navajas D (2008) Micropatterning of single endothelial cell shape reveals a tight coupling between nuclear volume in G1 and proliferation. Biophys J 94(12):4984–4995. doi:10.1529/biophysj.107.116863

Ronan W, Deshpande VS, McMeeking RM, McGarry JP (2012) Numerical investigation of the active role of the actin cytoskeleton in the compression resistance of cells. J Mech Behav Biomed Mater 14:143–157. doi:10.1016/j.jmbbm.2012.05.016

Rowat AC, Foster LJ, Nielsen MM, Weiss M, Ipsen JH (2005) Characterization of the elastic properties of the nuclear envelope. J Roy Soc Interf 2(2):63–69. doi:10.1098/rsif.2004.0022

Ruwhof C, Van Wamel J, Noordzij L, Aydin S, Harper J, Van Der Laarse A (2001) Mechanical stress stimulates phospholipase C activity and intracellular calcium ion levels in neonatal rat cardiomyocytes. Cell Calcium 29(2):73–83

Schuh E, Kramer J, Rohwedel J, Notbohm H, Muller R, Gutsmann T, Rotter N (2010) Effect of matrix elasticity on the maintenance of the chondrogenic phenotype. Tissue Eng Part A 16(4):1281–1290. doi:10.1089/ten.TEA.2009.0614

Schwartz MA, Schaller MD, Ginsberg MH (1995) Integrins: emerging paradigms of signal transduction. Annu Rev Cell Dev Biol 11:549–599. doi:10.1146/annurev.cb.11.110195.003001

Shemesh T, Bershadsky Alexander D, Kozlov Michael M (2012) Physical model for self-organization of actin cytoskeleton and adhesion complexes at the cell front. Biophys J 102(8):1746–1756. doi:10.1016/j.bpj.2012.03.006

Shemesh T, Geiger B, Bershadsky AD, Kozlov MM (2005) Focal adhesions as mechanosensors: a physical mechanism. Proc Natl Acad Sci USA 102(35):12383–12388

Solon J, Levental I, Sengupta K, Georges PC, Janmey PA (2007) Fibroblast adaptation and stiffness matching to soft elastic substrates. Biophys J 93(12):4453–4461

Somlyo AP, Somlyo AV (1994) Signal transduction and regulation in smooth muscle. Nature 372(6503):231–236. doi:10.1038/372231a0

Storm C, Pastore JJ, MacKintosh FC, Lubensky TC, Janmey PA (2005) Nonlinear elasticity in biological gels. Nature 435(7039):191–194. doi:10.1038/nature03521

Subramanian A, Lin H-Y (2005) Crosslinked chitosan: its physical properties and the effects of matrix stiffness on chondrocyte cell morphology and proliferation. J Biomed Mater Res Part A 75A(3):742–753. doi:10.1002/jbm.a.30489

Tan JL, Tien J, Pirone DM, Gray DS, Bhadriraju K, Chen CS (2003) Cells lying on a bed of microneedles: an approach to isolate mechanical force. Proc Natl Acad Sci USA 100(4):1484–1489

Tee S-Y, Fu J (2011) Cell shape and substrate rigidity both regulate cell stiffness. Biophys J 100(5):L25–L27. doi:10.1016/j.bpj.2010.12.3744

Thoumine O, Cardoso O, Meister JJ (1999) Changes in the mechanical properties of fibroblasts during spreading: a micromanipulation study. Eur Biophys J Biophys Lett 28(3):222–234

Tondon A, Hsu H-J, Kaunas R (2012) Dependence of cyclic stretch-induced stress fiber reorientation on stretch waveform. J Biomechan 45(5):728–735. doi:10.1016/j.jbiomech.2011.11.012

Vernerey FJ, Farsad M (2011) A constrained mixture approach to mechano-sensing and force generation in contractile cells. J Mechan Behav Biomed Mater 4(8):1683–1699. doi:10.1016/j.jmbbm.2011.05.022

Wang JHC (2000) Substrate deformation determines actin cytoskeleton reorganization: a mathematical modeling and experimental study. J Theor Biol 202(1):33–41

Wang N, Tolić-Nørrelykke IM, Chen J, Mijailovich SM, Butler JP, Fredberg JJ, Stamenović D (2002) Cell prestress. I. Stiffness and prestress are closely associated in adherent contractile cells. Am J Physiol Cell Physiol 282(3):C606–C616. doi:10.1152/ajpcell.00269.2001

Warshaw DM, Desrosiers JM, Work SS, Trybus KM (1990) Smooth muscle myosin cross-bridge interactions modulate actin filament sliding velocity in vitro. J Cell Biol 111(2):453–463. doi:10.1083/jcb.111.2.453

Yeung T, Georges PC, Flanagan LA, Marg B, Ortiz M, Funaki M, Zahir N, Ming W, Weaver V, Janmey PA (2005) Effects of substrate stiffness on cell morphology, cytoskeletal structure, and adhesion. Cell Motil Cytoskeleton 60(1):24–34. doi:10.1002/cm.20041

Zeng X, Li S (2011) Modelling and simulation of substrate elasticity sensing in stem cells. Comput Methods Biomech Biomed Eng 14(05):447–458

Zeng Y, Lai T, Koh CG, LeDuc PR, Chiam K-H (2011) Investigating circular dorsal ruffles through varying substrate stiffness and mathematical modeling. Biophys J 101(9):2122–2130